

# Optimization of cathode catalyst layer for direct methanol fuel cells Part II: Computational modeling and design

Fuqiang Liu, Chao-Yang Wang\*

*Electrochemical Engine Center (ECEC), Department of Materials Science and Engineering, The Pennsylvania State University,  
University Park, PA 16802, United States*

Received 19 March 2006; received in revised form 10 July 2006; accepted 11 July 2006  
Available online 7 September 2006

## Abstract

The cathode catalyst layer in direct methanol fuel cells (DMFCs) features a large thickness and mass transport loss due to higher Pt loading, and therefore must be carefully designed to increase the performance. In this work, the effects of Nafion loading, porosity distribution, and macro-pores on electrochemical characteristics of a DMFC cathode CL have been studied with a macro-homogeneous model, to theoretically interpret the related experimental results. Transport properties in the cathode catalyst layers are correlated to both the composition and microstructure. The optimized ionomer weight fraction (22%) is found to be much smaller than that in H<sub>2</sub> polymer electrolyte fuel cells, as a result of an optimum balance of proton transport and oxygen diffusion. Different porosity distributions in the cathode CLs are investigated and a stepwise distribution is found to give the best performance and oxygen concentration profile. Influence of pore defects in the CLs is discussed and the location of macro-pores is found to play a dual role in affecting both oxygen transport and proton conduction, hence the performance. The reaction zone is extended toward the membrane side and the proton conduction is facilitated when the macro-pores are near the gas diffusion layer.

© 2006 Elsevier Ltd. All rights reserved.

**Keywords:** Direct methanol fuel cell; Cathode; Catalyst layer; Porosity distribution; Modeling

## 1. Introduction

Both oxygen diffusion and proton conduction in thicker cathode CLs of direct methanol fuel cells (DMFCs) are more critical issues than in H<sub>2</sub> polymer electrolyte fuel cells (PEFCs). As shown experimentally in Part I of this study [1], electrode structure, ionomer and Pt distributions in a thick cathode CL have remarkable influence on its kinetic, ohmic and mass-transport characteristics. The aim of this *companion paper* is to theoretically examine the influence of ionomer, porosity, pores and their distributions on the performance of a thick cathode catalyst layer, thus providing guidance for MEA and CL design for portable DMFCs.

Computational modeling is widely used for basic understanding of transport and electrochemical phenomena in fuel cells, as well as for structure optimization. Notable work includes that of Springer et al. [2], and Bernardi and Verbrugge [3], whose

models are used to predict water transport through the membrane. Fuller and Newman [4], Nguyen and White [5], Um and Wang [6], and Gurau et al. [7] developed multidimensional models to address heat and water management in H<sub>2</sub> PEFCs. In these models, the active CL is not the main point of interest, but rather simplified as an infinitely thin film interface. There are only few detailed models specifically developed for PEFC CLs [8–11]. In these models, optimization of the cathode CLs in H<sub>2</sub> PEFCs was conducted to determine the optimal Nafion content, Pt loading and CL thickness, by assuming that the Nafion content and Pt loading were uniformly distributed in the CLs. Recently, improvement in PEFC cathode CL performance was realized by introducing concepts involving functionally graded Pt loadings or Nafion contents [12–14]. However, only 1D models were developed in their work and the porosity distribution in the CLs has not been studied. To date, DMFC cathode CL optimization and modeling under portable operating conditions have not been attempted.

In this paper, a macro-homogeneous model is developed, where the properties and variables of each phase are averaged over a representative elementary volume. Further, a 2D model

\* Corresponding author. Tel.: +1 814 863 4762; fax: +1 814 863 4848.  
E-mail address: [cwx31@psu.edu](mailto:cwx31@psu.edu) (C.-Y. Wang).

for oxygen and proton transport in the CL has been developed, where the CL is described using porosity, interfacial area per unit volume, effective conductivity and diffusivity through a porous medium. The effective conductivity and diffusivity are corrected as functions of ionomer fraction and porosity in the CL. This model enables direct analysis of not only the influence of ionomer and porosity distribution but also the effect of the location of macro-pore in the CL on the electrochemical characteristics. The present study is only concerned with the CL on the cathode side, with methanol crossover effect on DMFC cathode performance to be explored in future publication.

## 2. Numerical model

The cathode CL consists of a matrix of carbon and Pt catalyst, with ionomer and pores distributed within. In the cathode half-reaction, oxygen is reduced to produce water at the triple-phase boundary. Assumptions made in this study are: (1) the system is assumed to be isothermal and at steady state, (2) at the reaction interface, O<sub>2</sub> diffusion resistance through the ionomer film is ignored due to its small thickness (i.e. ~5 nm), (3) product water is assumed to be removed efficiently, thus does not affect the diffusion of O<sub>2</sub>, and (4) the intrinsic proton conductivity is taken as a constant due to sufficient hydration in a DMFC environment.

### 2.1. Governing equations

Similarly to Part I [1], H<sub>2</sub> PEFCs are used to evaluate the cathode performance and methanol crossover or the anode overpotential is not considered here. An optimized cathode CL structure in DMFCs should have a good balance between proton conduction and oxygen mass transport through its thickness. The governing equations can be written as

$$\nabla(\kappa_e \nabla \phi_e) + aj = 0 \quad (1)$$

and

$$\nabla(D_{\text{CL}}^{\text{O}_2, \text{eff}} \nabla c_{\text{O}_2}) + \frac{aj}{4F} = 0 \quad (2)$$

where  $j$ ,  $\kappa_e$ ,  $\phi_e$ ,  $a$ ,  $D_{\text{CL}}^{\text{O}_2, \text{eff}}$ ,  $c_{\text{O}_2}$  and  $F$  are the transfer current, effective ionic conductivity, electrolyte potential, electrochemical area (ECA) per unit of electrode volume, effective oxygen diffusivity, oxygen concentration and Faraday constant, respectively. Eq. (1) describes proton conservation through the electrolyte phase, and Eq. (2) governs oxygen diffusion through the CL. The second term in both equations represents a source/sink term, accounting for the electrochemical reaction in the cathode CL.

The transfer current  $j$ , or the rate of ORR is governed by the Tafel kinetics as follows:

$$j = -i_0 \frac{c_{\text{O}_2}}{c_{\text{O}_2, \text{ref}}} \exp\left(-\frac{\alpha_c F}{RT} \eta\right) \quad (3)$$

where  $i_0$ ,  $c_{\text{O}_2, \text{ref}}$ ,  $\alpha_c$  and  $\eta$  are the exchange current density, reference oxygen concentration, cathode transfer coefficient and

overpotential. The overpotential,  $\eta$ , is defined as

$$\eta = \phi_s - \phi_e - V_{\text{oc}} \quad (4)$$

where  $\phi_s$  and  $\phi_e$  stand for potentials of electronic phase and electrolyte at the reaction site, respectively.  $V_{\text{oc}}$  is the thermodynamic open circuit potential of cathode at the operation temperature. If we assume that the Pt/C phase provides a sufficiently large electronic conductivity, which is reasonable in practice for common loading of Pt/C; then the entire CL has a uniform electronic phase potential, i.e.,  $(\partial \phi_s / \partial x) = 0$ . Letting  $\eta = -\phi$ , we have the following relation:

$$\frac{\partial \phi_e}{\partial x} = \frac{\partial(\phi_s - V_{\text{oc}} - \eta)}{\partial x} = \frac{\partial(-\eta)}{\partial x} = \frac{\partial \phi}{\partial x} \quad (5)$$

Substituting Eqs. (5) and (3) into Eqs. (1) and (2), respectively, the governing equations can be rewritten as

$$\nabla(\kappa_e \nabla \phi) - ai_0 \frac{c_{\text{O}_2}}{c_{\text{O}_2, \text{ref}}} \exp\left(\frac{\alpha_c F}{RT} \phi\right) = 0 \quad (6)$$

and

$$\nabla(D_{\text{CL}}^{\text{O}_2, \text{eff}} \nabla c_{\text{O}_2}) - \frac{ai_0}{4F} \frac{c_{\text{O}_2}}{c_{\text{O}_2, \text{ref}}} \exp\left(\frac{\alpha_c F}{RT} \phi\right) = 0 \quad (7)$$

Based on the reference that the membrane phase potential is zero at the membrane/cathode interface, the cathode potential is then obtained by

$$V_{\text{cath}} = V_{\text{oc}} + \eta = V_{\text{oc}} - \phi \quad (8)$$

According to the percolation theory [8,9,12], the effective proton conductivity and oxygen diffusivity in the CL can be obtained through the following equation:

$$\kappa_e = \kappa_{e,0} \left(\frac{\varepsilon_e - X_0}{1 - X_0}\right)^2 \quad (9)$$

$$D_{\text{CL}}^{\text{O}_2, \text{eff}} = D_{\text{g}}^{\text{O}_2} \left(\frac{\varepsilon_{\text{CL}} - X_0}{1 - X_0}\right)^2 \quad (10)$$

where  $\kappa_{e,0}$ ,  $\varepsilon_{\text{CL}}$ ,  $\varepsilon_e$ ,  $X_0$ , and  $D_{\text{g}}^{\text{O}_2}$  are the intrinsic proton conductivity of fully hydrated polymer, porosity, electrolyte volume fraction in the CL, percolation critical value, and bulk oxygen diffusivity, respectively.

According to Part I of this series [1], DMFC cathode Pt loading is about 1.2–1.5 mg cm<sup>-2</sup>, corresponding to a CL thickness about 25–30 μm. The porosity  $\varepsilon_{\text{CL}}$  can thus be estimated by knowing the densities of Pt, carbon and Nafion [1]. Similarly, the ionomer volume fraction in the CL is calculated by the following equation, assuming that Pt/C catalyst and ionomer are well mixed

$$\varepsilon_e = (1 - \varepsilon_{\text{CL}}) \times \frac{((1.5 \times \text{SW} \times R_{I/C}) / \rho_{\text{Nafion}})}{(1/\rho_{\text{Pt}}) + (1.5/\rho_c) + ((1.5 \times \text{SW} \times R_{I/C}) / \rho_{\text{Nafion}})} \quad (11)$$

where  $\rho_{\text{Nafion}}$ ,  $\rho_{\text{Pt}}$ , and  $\rho_c$  are the density of hydrated Nafion, Pt and carbon, respectively. SW is the swelling degree of dry ionomer upon hydration by weight (120%). From the above

Table 1  
Parameters used in the simulation of the cathode catalyst layer

Parameters	Value
Intrinsic proton conductivity of fully hydrated polymer, $\kappa_{e,0}$ (S/cm)	0.1
Reactive area per volume, $a$ ( $\text{m}^2/\text{m}^3$ )	400
Oxygen diffusion coefficient, $D_g^{\text{O}_2}$ ( $\text{m}^2/\text{s}$ )	$1 \times 10^{-5}$
Transfer coefficient of cathode, $\alpha_c$	1.0
Reference exchange current density, $i_0$ ( $\text{A}/\text{m}^2$ )	$1 \times 10^{-5}$
Reference oxygen concentration of cathode kinetics, $c_{\text{O}_2,\text{ref}}$ ( $\text{mol}/\text{m}^3$ )	8.825
Air pressure in gas channel inlet, $p$ (kPa)	100
Operating temperature, $T$ ( $^\circ\text{C}$ )	60
Thickness of the GDL, $\Delta X_{\text{GDL}}$ ( $\mu\text{m}$ )	300
Tortuosity of the GDL, $\tau_{\text{GDL}}$	4
Porosity of the GDL, $\varepsilon_{\text{GDL}}$	0.4
Swelling degree of ionomer upon hydration by weight, SW	1.2
Percolation critical value, $X_0$	0.13
Stoichiometric parameter, $S$	0.65
Thermodynamic open circuit potential at $60^\circ\text{C}$ and ambient pressure, $E_{\text{oc}}$ (V)	1.19
Density of Nafion, $\rho_{\text{Nafion}}$ ( $\text{g}/\text{cm}^3$ )	1.9
Density of Pt, $\rho_{\text{Pt}}$ ( $\text{g}/\text{cm}^3$ )	21.5
Density of carbon, $\rho_c$ ( $\text{g}/\text{cm}^3$ )	2.0

equations, it can be seen that increasing ionomer content leads to reduction of porosity and effective oxygen diffusivity in the CL, but to an increase of the effective proton conductivity. In the case of non-uniform porosity distribution in the CL, the effective proton conductivity and oxygen diffusivity at different locations along the CL can be calculated using Eqs. (9) and (10).

At a certain Nafion loading, ECA per unit volume of solid (i.e. Pt and ionomer) in the CL can be safely assumed to be constant; consequently, the ECA per unit volume of the electrode (i.e. solid plus voids),  $a$ , should be linearly proportional to the local solid fraction of Pt/Nafion composite in the catalyst layer, namely

$$a = a_0 \frac{1 - \varepsilon_{\text{CL}}}{1 - \varepsilon_0} \quad (12)$$

where  $a_0$  is the reference ECA per unit volume of the electrode at porosity  $\varepsilon_0$  in the catalyst layer. All the parameters used are listed in Table 1 and the governing equations in a multi-dimensional situation are solved by the finite volume method [15].

## 2.2. Boundary conditions

A 2D computational domain, as shown Fig. 1, is symmetric in  $y$  direction. The boundary conditions in  $y$  directions are

$$y = 0, \quad y = y_L, \quad \frac{\partial c_{\text{O}_2}}{\partial y} = 0, \quad \frac{\partial \phi}{\partial y} = 0 \quad (13)$$

At the left boundary (bonded with the membrane), it can be written as

$$x = 0, \quad \frac{\partial c_{\text{O}_2}}{\partial x} = 0, \quad -\kappa_e \frac{\partial \phi}{\partial x} = I \quad (14)$$

while at the right boundary (connected with GDL), oxygen concentration is assumed to be constant, which is dependent on

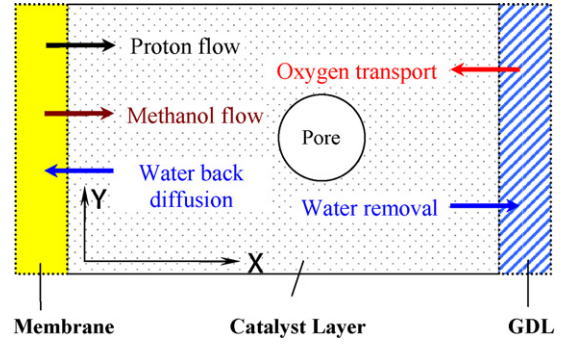


Fig. 1. Schematic diagram of transport process in cathode CL of a DMFC.

operating current density

$$x = x_L, \quad c_{\text{O}_2} = c_{\text{O}_2,0}, \quad \frac{\partial \phi}{\partial x} = 0 \quad (15)$$

Oxygen concentration drop across GDL is included in the oxygen concentration boundary condition,  $c_{\text{O}_2,0}$ , given by [16]

$$c_{\text{O}_2,0} = S c_{\text{O}_2,\text{inlet}} - \frac{I \Delta X_{\text{GDL}}}{4 F D_{\text{g,GDL}}^{\text{O}_2,\text{eff}}} \quad (16)$$

where  $\Delta X_{\text{GDL}}$  represents the thickness of GDL,  $D_{\text{g,GDL}}^{\text{O}_2,\text{eff}}$  is effective diffusion coefficient in GDL,  $c_{\text{O}_2,\text{inlet}}$  is the inlet oxygen concentration in the gas channel, and  $S$  the stoichiometric parameter, which is the ratio of oxygen concentration at the interface of GDL/gas channel to that at the inlet.  $S = 1$  corresponds to a large air stoichiometry, where the concentration gradient in the gas channel is eliminated; when the stoichiometry is small,  $S$  is less than 1. The porosity  $\varepsilon$  and tortuosity  $\tau$  are employed to obtain the effective diffusivities in porous media [16]

$$D_{\text{g,GDL}}^{\text{O}_2,\text{eff}} = D_g^{\text{O}_2} \frac{\varepsilon_{\text{GDL}}}{\tau_{\text{GDL}}} \quad (17)$$

Two scenarios are simulated: one in the absence of macro-pores (thus reduced to a 1D problem) and the other in the presence of pores.

## 3. Results and discussion

### 3.1. Effect of Nafion content on performance

Fig. 2 shows the effect of Nafion loading on the cathode performance at  $60^\circ\text{C}$  under fully humidified air at ambient pressure. A stoichiometric factor  $S = 0.65$  is used, corresponding to a low air stoichiometry. At  $I/C$  ratios of 1:1.8, 1:2.1 and 1:2.4, porosities of the CL are estimated to be about 0.18, 0.25, and 0.33, and the electrolyte volume fractions are estimated to be about 0.31, 0.27, and 0.24, respectively. The effect of Nafion loading on the cathode performance is consistent with the experimental results in Part I [1]. Cathode 3 with  $I/C$  ratio of 1:2.4 shows the highest limiting current density around  $500 \text{ mA cm}^{-2}$ , while those of the other two are much smaller, around 450 and  $480 \text{ mA cm}^{-2}$  for cathode 1 and 2, respectively. The difference between the three cathodes is diminishing with decreasing current density. According to Uchida et al. [17], the volume of secondary pores

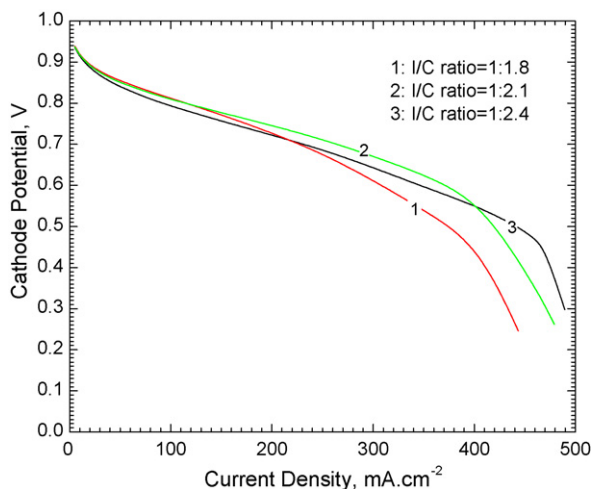


Fig. 2. Effect of Nafion content in the cathode CL on the polarization behavior of MEAs at 60 °C using fully humidified air at ambient pressure.

in the CL, formed between agglomerates, increases linearly with the decrease of Nafion loading. This indicates that lower Nafion fraction (cathode 3) leads to larger pore volume, thus better mass transport in CL. Cathode 2 performs better than the other two in the moderate current region, i.e., between 150 and 400 mA cm<sup>-2</sup>. Further increase of Nafion loading only slightly improves the performance at low current densities, since higher Nafion fraction leads to a reduction of ohmic losses. However, when current density increases (>200 mA cm<sup>-2</sup>), the O<sub>2</sub> transport limitation becomes more severe, reducing the performance. *I/C* ratios of 1:1.8, 1:2.1, and 1:2.4 correspond to Nafion weight fractions of 25%, 22%, and 20%, respectively, which are much smaller than those in H<sub>2</sub> PEMFCs, where the peak performance is usually achieved at much higher Nafion weight fraction between 30% and 40% [18–22]. This is because that the optimum Nafion loading depends on Pt loading. Higher Pt loading in the CLs of DMFCs requires smaller optimum Nafion loading, since a larger porosity is needed for oxygen supply and water removal through a thicker CL. The finding of the optimal ionomer fraction at 22% for DMFC cathodes is in excellent agreement with experimental data shown in Part I [1] (i.e. MEA-F).

Simulation results of oxygen concentration profile and overpotential distribution in the three CLs are shown in Fig. 3a and b at 150 and 400 mA cm<sup>-2</sup>, respectively. Clearly, the consequence of increasing Nafion loading is two-fold: oxygen transport becomes worse and simultaneously ohmic resistance decreases significantly. The cathode performance is determined by two competing factors, i.e., oxygen transport and ionic resistance in the CL. Therefore an optimized performance is achieved through a good balance of the two at certain Nafion weight fraction. Reducing Nafion content always makes mass transport easier, as demonstrated in the figures that lower Nafion fraction reduces concentration drop through the CL, pushing the reaction zone towards the membrane. However, lower Nafion content increases the potential drop across the CL at lower current density as shown for CL 3 in Fig. 3a. In this case the rate of oxygen diffusion is relatively large compared to the electro-

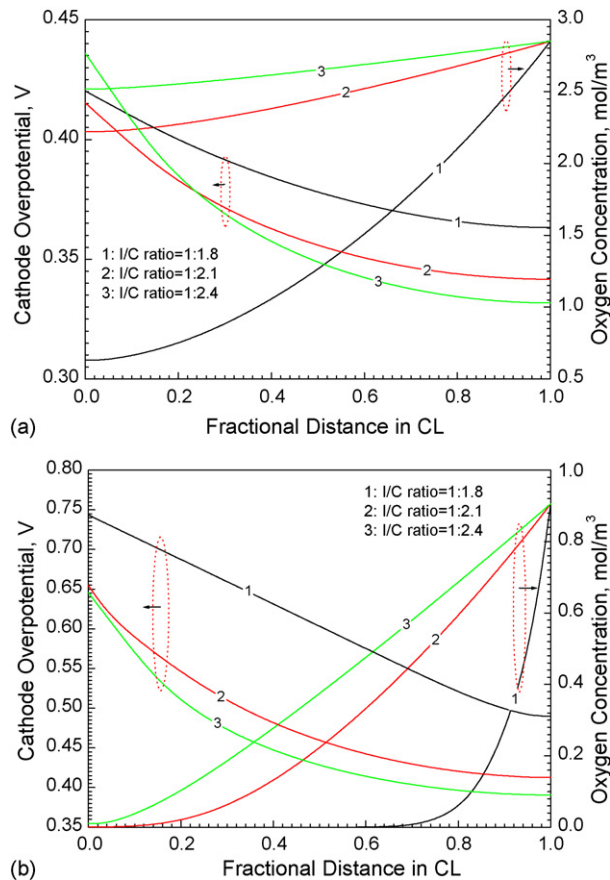


Fig. 3. Distribution of oxygen concentration and cathode overpotential at (a) 150 mA cm<sup>-2</sup> and (b) 400 mA cm<sup>-2</sup> in the cathode CLs. The operating condition is 60 °C, using fully humidified air and ambient pressure.

chemical reaction rate. At higher current density, a large amount of oxygen is consumed, thus making mass transport the limiting step. Inspection of the oxygen concentration profile in Fig. 3b reveals that up to 60–70% of the catalytic sites in the CL1 experiences zero oxygen concentration and could not contribute to the ORR. The overpotential at the front interface,  $\eta_0$ , which is the indicator of the total voltage loss, is about 100 mV larger at *I/C* ratio of 1:1.8 than the other two cases, indicating that oxygen transport dominates over the ionic resistance in determining the cathode performance in this case.

### 3.2. Effect of porosity distribution on cathode performance

In order to study the porosity distribution effect solely, other parameters, including the *I/C* ratio, thickness and ECA are set constant. Six cathode CLs with different porosity distributions are investigated in this study. In Fig. 4, (A) has a uniform porosity distribution; the porosity distributions in the CLs of (B), (C) and (F) are stepwise; and (D) and (E) are linear. All porosity distributions have the identical average porosity of 25%. Although the local ECA per unit volume depends on the local porosity,  $\varepsilon_{CL}$ , the overall ECA obtained by integrating Eq. (12) through the whole CL is constant.

Fig. 5 compares the performance of the six cathode CLs (*I/C* ratio = 1:2.1) with different porosity distributions. Cathode (A)

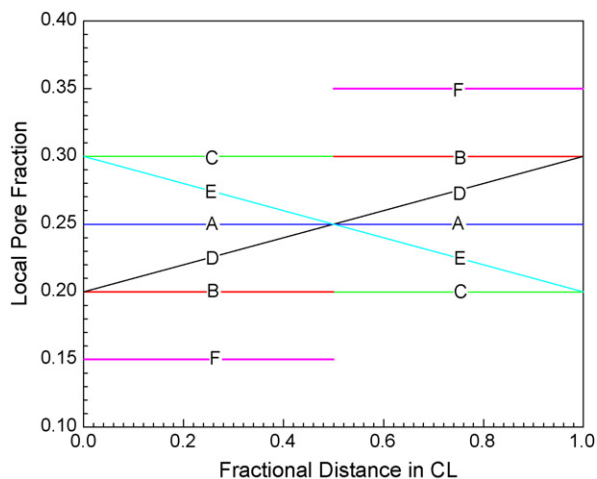


Fig. 4. Porosity distribution of the six different cathode CL structures: (A) uniform; (B), (C) and (F) are step-wise; and (D) and (E) are linear distribution.

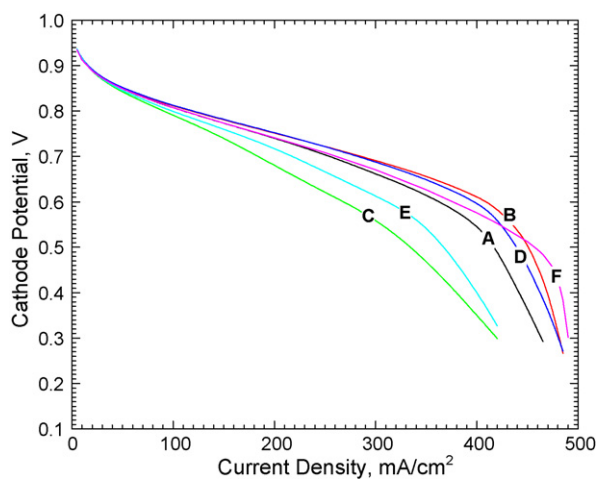


Fig. 5. Performances for different cathode CLs ( $I/C$  ratio = 1:2.1) at 60 °C. The porosity distributions of these cathode CLs are depicted in Fig. 4.

is the baseline, which has a uniform porosity distribution of 25% along the thickness. First, by comparing the performances of the baseline with cathodes (B–E), which have either 20% or 30% porosity at the membrane/CL or GDL/CL interfaces, it is clear that higher porosity near the interface of CL/GDL is helpful for  $O_2$  transport and water removal. All these CLs perform almost identically when the current density is smaller than

$50 \text{ mA cm}^{-2}$ , but the difference becomes larger with increasing current density. At  $400 \text{ mA cm}^{-2}$  the cathode potential of (B) is 60 and 260 mV larger than (A) and (C), respectively. The reason is evident from Fig. 6a–c, which show the  $O_2$  concentration profiles through the catalyst layer. At small current density ( $50 \text{ mA cm}^{-2}$ ),  $O_2$  concentration distributions of all the CLs are more homogeneous, with small variations along the thickness.

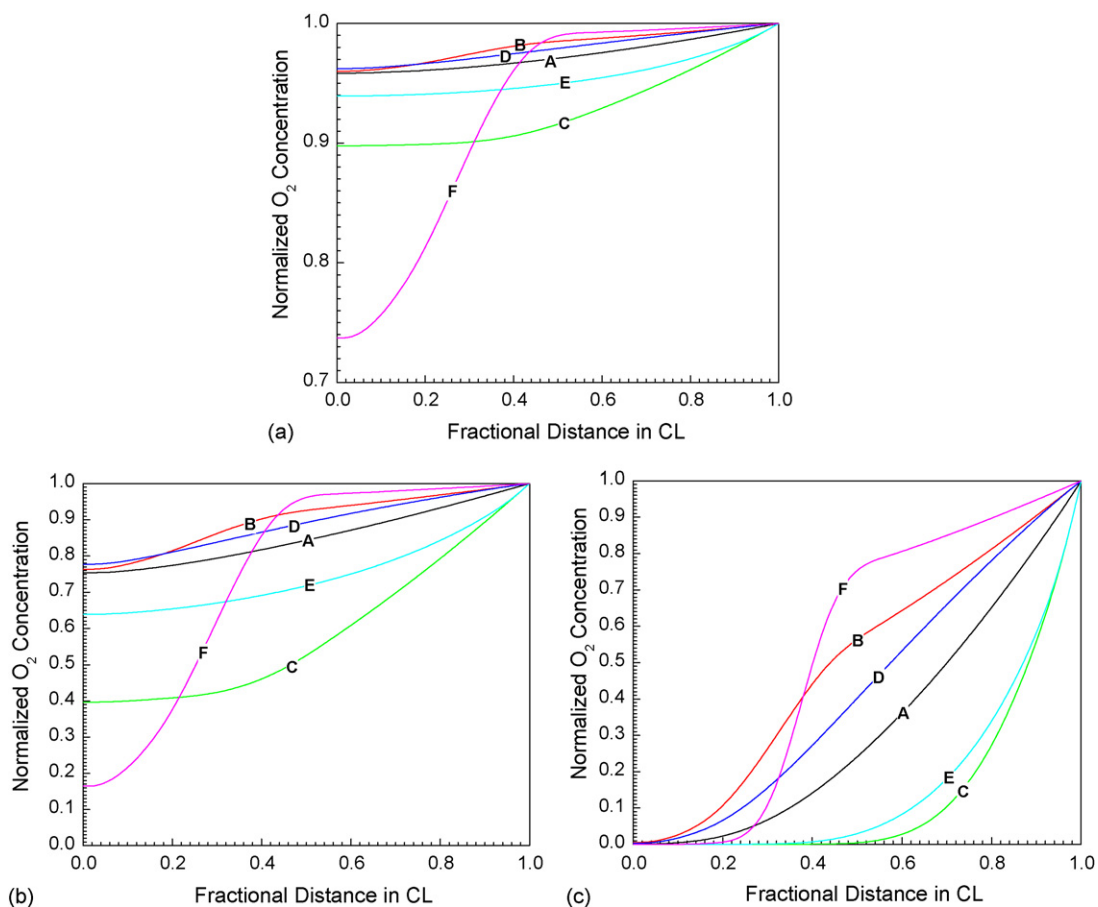


Fig. 6. Oxygen concentration distributions in the CLs A ~ E ( $I/C$  ratio = 1:2.1) at current densities of (a)  $50 \text{ mA cm}^{-2}$ , (b)  $150 \text{ mA cm}^{-2}$ , and (c)  $400 \text{ mA cm}^{-2}$ .

However, at high current density ( $400 \text{ mA cm}^{-2}$ ), there are significant  $\text{O}_2$  concentration drops in these CLs: (B) exhibits a more even distribution than (D) and (A); (C), a reverse configuration to (B), has the lowest  $\text{O}_2$  concentration throughout the whole CL, and there are significant fractions (up 50%) of the CLs of (C) and (E) operated under  $\text{O}_2$  depletion. For the same porosities at the membrane/CL and GDL/CL interfaces, stepwise porosity distribution (B) has better performance and oxygen distribution than the linear distribution (D).

Second, to further explore the effect of stepwise distribution, (B) and (F) are compared, both of which have the stepwise distribution and identical average porosity. In the half sublayer near the GDL, because of larger porosity (35%), (F) has higher  $\text{O}_2$  concentration than (B) as shown in Fig. 6; however, it has larger ohmic drop due to smaller ionomer fraction to conduct protons. In the half sublayer near the membrane,  $\text{O}_2$  concentration in (F) decreases dramatically far below that of (B) and it cannot be compensated by its smaller ionic resistance. So the net result is that (B) has better performance than (F) at almost all the current densities, except that the current density is very high (larger than  $450 \text{ mA cm}^{-2}$  in Fig. 5), where oxygen transport dominates over ohmic loss.

### 3.3. Influence of macro-pores

During CL fabrication process, some macro-pores can be formed due to insufficient mixing, as shown in the TEM image in Part I [1]. These can be as large as several  $\mu\text{m}$  in diameter. Supposing that there is a  $10\text{-}\mu\text{m}$ -diameter pore in a cathode CL of  $30\text{-}\mu\text{m}$  thick and  $30\text{-}\mu\text{m}$  wide, the influence of its position on cathode performance, proton conduction and  $\text{O}_2$  concentration distribution is investigated here in three cases: 1–3, corresponding to its location near the GDL, in the middle of the CL, and near the membrane, respectively. The computational domain and locations of the pores in the three cases are shown in Figs. 9–11, respectively. Mathematical description of a macro-pore in the CL includes: no electrochemical reaction; effective oxygen diffusivity equal to the bulk value; and effective proton conductivity of zero. Obviously the macro-pore cannot contribute to electrochemical reaction, but it will influence proton conduction and  $\text{O}_2$  distribution profile in the CL.

The location of pores plays an important role in affecting the performance, as shown in Fig. 7. Cases 1 and 2 have almost identical cathode performance up to  $\sim 350 \text{ mA cm}^{-2}$ , beyond which case 1 shows better performance and larger limiting current density. For case 3 with the macro-pore near the membrane side, the cathode potential reduces from 15 to 55 mV comparing to case 1 between 100 and  $400 \text{ mA cm}^{-2}$ .

The performance gain of case 1 over the other two cases can be explained in term of both proton conduction and oxygen transport. Fig. 8 shows the total voltage loss (overpotential) profile along the CL/PEM interface for three different cases at  $100 \text{ mA cm}^{-2}$ , where cathode performances are dominated by proton transport. The cathode potential is obtained by an average along the interface. The overpotential distributions of cases 1 and 2 along the interface are relative uniform; however, the

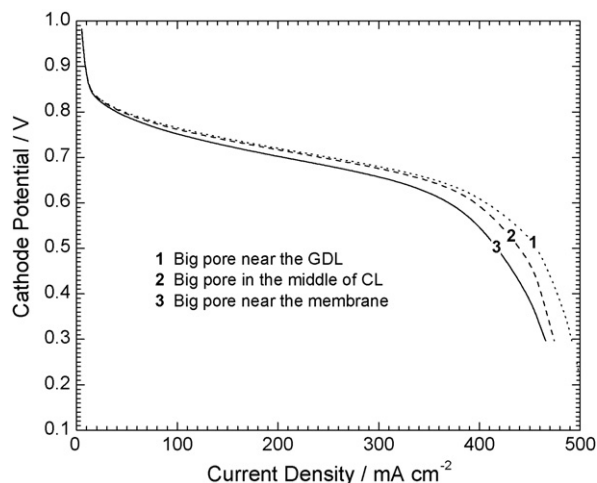


Fig. 7. Cathode performances for three cases ( $I/C$  ratio = 1:2.1): (1) the pore near the GDL, (2) in the middle of CL, and (3) near the membrane. The diameter of the pore is  $10 \mu\text{m}$  and the thickness of cathode CL is  $30 \mu\text{m}$ .

overpotential bulges up in the middle for case 3, much higher than the other two cases. This is because protons transport over the macro-pore through the CL with more difficulty for case 3 with a macro-pore near the membrane, as proton conduction in the pores is impossible. Since a constant current density at the CL/PEM interface is assumed in Eq. (14), the overpotential, therefore, has to increase to sustain the desired current, especially in the middle area facing the pore.

Oxygen concentration contours of the three cases at  $400 \text{ mA cm}^{-2}$  are shown in Figs. 9–11, respectively. Inside the macro-pore gases diffuse much faster than in the surrounding area, so the oxygen concentration is relatively constant there and higher than in the area around the pore. Therefore, macro-pores in a CL play a dual role. First, in the space between the front surface of the pore and the GDL, oxygen concentration profile lags compared to the surrounding area, since there is no oxygen consumed within the pore and the diffusion lacks driving force. Second, in the space between the back surface and the membrane, the oxygen concentration profile is pushed forward

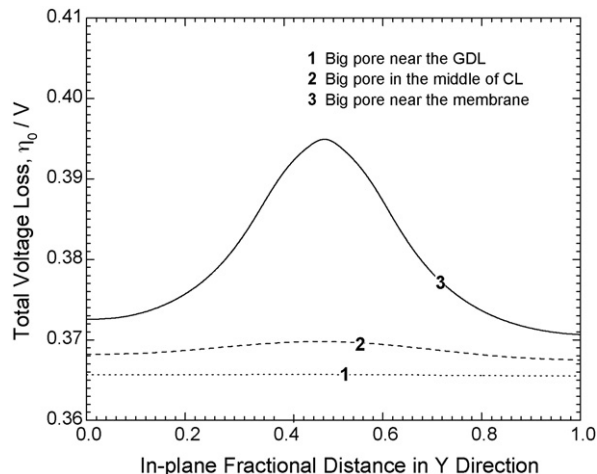


Fig. 8. Total voltage loss distribution along the CL/PEM interface at  $100 \text{ mA cm}^{-2}$  for three different cases.

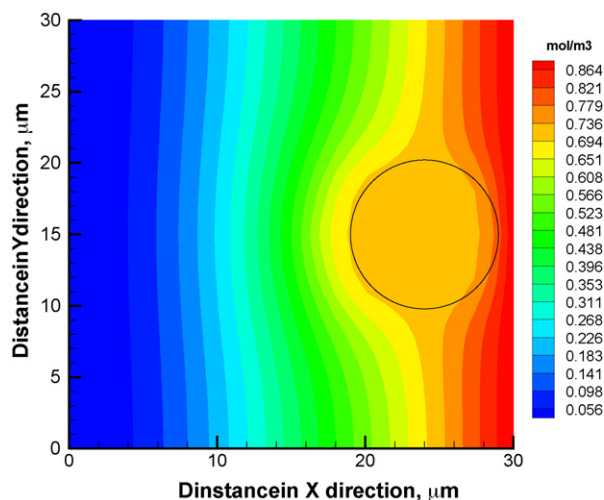


Fig. 9. Oxygen concentration contour in the cathode CL at  $400 \text{ mA cm}^{-2}$  when a macro-pore (indicated by the circle) is near the GDL side (case 1).

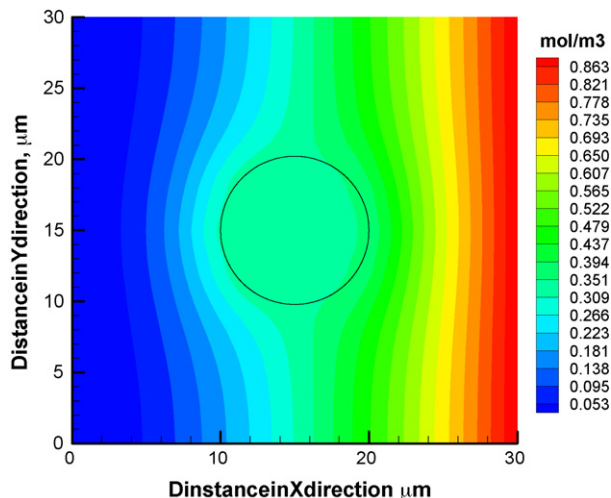


Fig. 10. Oxygen concentration contour in the cathode CL at  $400 \text{ mA cm}^{-2}$  when a macro-pore (indicated by the circle) is in the middle of the CL (case 2).

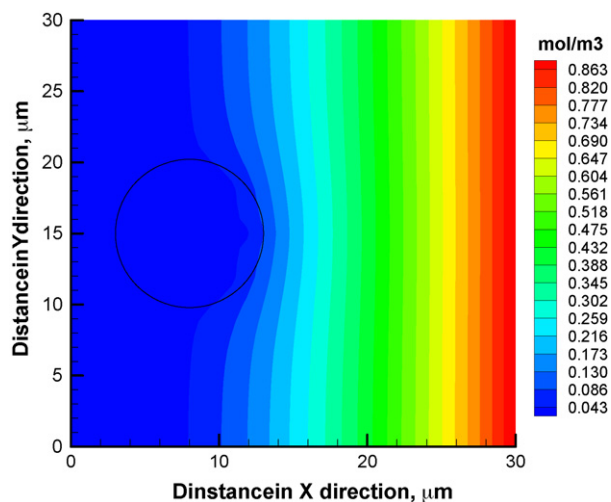


Fig. 11. Oxygen concentration contour in the cathode CL at  $400 \text{ mA cm}^{-2}$  when a macro-pore (indicated by the circle) is near the membrane side (case 3).

toward the membrane because of the higher  $\text{O}_2$  diffusivity in the pore. To provide more active Pt sites in the CL for operation at higher  $\text{O}_2$  concentration, the space between the front surface and GDL must be shrunk or the space between the back surface and the membrane must be expanded. For this reason, case 1 shows better performance than those of cases 2 and 3. In Fig. 9 where the pore is near the GDL side, it is clear that the  $\text{O}_2$ -depletion area shrinks and the reaction zone is extended toward the inside facing the membrane.

#### 4. Summary

DMFC cathode CL features a large thickness and mass transport loss and must be carefully considered in order to optimize its performance. At low air stoichiometry, ambient pressure and low temperature, both diffusion of  $\text{O}_2$  and conduction of proton in the thick cathode CL layer are more critical. Optimized performance is achieved through a good balance of the two factors at medium Nafion weight fraction (22 wt.%) in CL, in good agreement with the experimental finding of Part I [1] (i.e. MEA-F). The smaller optimum Nafion fraction in this study than reported values (around 35 wt.%) in  $\text{H}_2$  PEFCs is intended to provide more pore volume in the CL, thus improving the  $\text{O}_2$  diffusion. CL structure with higher porosity near the GDL is helpful for  $\text{O}_2$  transport and byproduct removal. The CL with stepwise porosity distribution, with higher porosity near the GDL and lower one near the membrane, performs better than that with linear distribution, especially at high current density. This is because it exhibits a healthier  $\text{O}_2$  distribution in the CL, thus extending the reaction zone forward toward the membrane side. The position of macro-pores plays an important role in affecting proton conduction and oxygen transport in the CL, hence the performance. A cathode CL has superior performance and favorable oxygen concentration profile when the pore is near the GDL.

#### References

- [1] F.Q. Liu, C.Y. Wang, *Electrochim. Acta*, 2006, doi:10.1016/j.electacta.2006.08.003, this volume.
- [2] T.E. Springer, T.A. Zawodzinski, S. Gottesfeld, *J. Electrochem. Soc.* 138 (1991) 2334.
- [3] D.M. Bernardi, M.W. Verbrugge, *J. Electrochem. Soc.* 139 (1992) 2477.
- [4] T.F. Fuller, J. Newman, *J. Electrochem. Soc.* 140 (1993) 1218.
- [5] T.V. Nguyen, R.E. White, *J. Electrochem. Soc.* 140 (1993) 2178.
- [6] S. Um, C.Y. Wang, C.S. Chen, *J. Electrochem. Soc.* 147 (2000) 4485.
- [7] V. Gurau, H.T. Liu, S. Kakac, *AIChE J.* 44 (1998) 2410.
- [8] M. Eikerling, A.A. Kornyshev, *J. Electroanal. Chem.* 453 (1998) 89.
- [9] M. Eikerling, A.A. Kornyshev, *J. Electroanal. Chem.* 475 (1999) 107.
- [10] C. Marr, X.G. Li, *J. Power Sources* 77 (1999) 17.
- [11] D.T. Song, Q.P. Wang, Z.S. Liu, T. Navessin, M. Eikerling, S. Holdcroft, *J. Power Sources* 126 (2004) 104.
- [12] Q.P. Wang, M. Eikerling, D.T. Song, Z.S. Liu, T. Navessin, Z. Xie, S. Holdcroft, *J. Electrochem. Soc.* 151 (2004) A950.
- [13] O. Antoine, Y. Bultel, P. Ozil, R. Durand, *Electrochim. Acta* 45 (2000) 4493.
- [14] D. Song, Q. Wang, Z. Liu, T. Navessin, S. Holdcroft, *Electrochim. Acta* 50 (2004) 731.
- [15] S.V. Pantankar, *Numerical Heat Transfer and Fluid Flow*, Hemisphere, Washington, DC, 1980.

- [16] G.Q. Wang, Ph.D. Dissertation, Pennsylvania State University, University Park, Pennsylvania, 2003.
- [17] M. Uchida, Y. Aoyama, N. Eda, A. Ohta, J. Electrochem. Soc. 142 (1995) 4143.
- [18] E. Antolini, L. Giorgi, A. Pozio, E. Passalacqua, J. Power Sources 77 (1999) 136.
- [19] E. Passalacqua, F. Lufrano, G. Squadrito, A. Patti, L. Giorgi, Electrochim. Acta 46 (2001) 799.
- [20] J.M. Song, S.Y. Cha, W.M. Lee, J. Power Sources 94 (2001) 78.
- [21] Z. Qi, A. Kaufman, J. Power Sources 113 (2003) 37.
- [22] G. Sasikumar, J.W. Ihm, H. Ryu, J. Power Sources 132 (2004) 11.